Initial stages of Cu epitaxy on Ni(100): Postnucleation and a well-defined transition in critical island size

Bert Müller, Lorenz Nedelmann, Bjørn Fischer, Harald Brune, and Klaus Kern
Institut de Physique Expérimentale, EPF Lausanne, CH-1015 Lausanne, Switzerland
(Received 12 August 1996)

We present a comprehensive study of the nucleation kinetic of Cu on Ni(100) using variable-temperature scanning tunneling microscopy. The analysis of the saturation island density as a function of substrate temperature and deposition rate reveals that the smallest stable island abruptly changes from a dimer to a tetramer. From the Arrhenius plot, the migration barrier $E_m=(0.35\pm0.02)$ eV, as well as the dimer bond energy $E_b=(0.46\pm0.19)$ eV, has been deduced. For low ratios between the migration constant D and flux R ($D/R<10^4$), nucleation and island growth take place not only during, but also after deposition. In this postnucleation regime, the final island density and island size distribution are no more determined by the competition between flux and monomer migration, but solely by the monomer concentration present immediately after deposition. Therefore, the island density becomes independent of substrate temperature and flux, and the scaled island size distribution closely resembles that of statistic growth (adatom smallest stable island). The experimental results are compared with simulations using rate equations. [S0163-1829(96)10948-6]

I. INTRODUCTION

Quantitative understanding of the nucleation and growth of heteroepitaxial films is challenging both from a fundamental and a technological point of view, as it establishes how the film morphology is related to the growth conditions. The fundamental processes during submonolayer growth involve adatom diffusion, nucleation, aggregation, and coalescence, all being controlled by the external parameters of deposition rate and substrate temperature. Proceeding with the deposition on a defect-free substrate, the adatoms can migrate, meet further adatoms, and form nuclei. These nuclei either dissociate (subcritical size $<i$) or, for the critical ones (size i), grow to stable islands upon the incorporation of one extra atom. These islands then continue to grow and at a coverage between 0.1 and 0.2 monolayers (ML), the island density usually saturates, just before coalescence of the islands sets in. The dependence of the saturation island density on substrate temperature and flux can be used to extract microscopic parameters such as activation barriers for surface migration and dimer dissociation by means of mean-field nucleation theory.[1,2]

The saturation island density can be measured by several surface-sensitive techniques, such as electron microscopy,[2] electron diffraction,[3] helium atom diffraction,[4] and scanning tunneling microscopy (STM).[5–12] With respect to STM, the other methods have certain disadvantages. The resolution of electron microscopy is not sufficient to image high island densities ($n_x>10^{-3}$) and small islands of a few atoms. Electron diffraction and helium atom diffraction are methods in reciprocal space; therefore, they require a certain knowledge about the island size and separation distributions in order to extract distances and densities in real space. In addition, they have difficulties detecting islands at small coverages ($\Theta<0.1$ ML). The averaging character of these diffraction techniques yields a high statistical significance, on the one hand, and at the same time it is a disadvantage since areas with defects such as steps are included in the average. For these reasons, STM has gained attraction for nucleation studies. In particular, through the availability of variable-temperature STM for temperatures below room temperature[5,6] the very early stages of nucleation could be addressed on the atomic level.

One of the first systematic nucleation studies by means of STM on metal surfaces has been carried out by Stroscio *et al.*, who investigated the homoepitaxial growth on Fe(100) at substrate temperatures above 300 K.[7] They derived the migration barrier from the temperature dependence of the saturation island density using nucleation theory in assuming a critical nucleus size of 1. Later on, the sizes of the critical nuclei were determined by the scaling behavior of the island size distribution.[13] Brune *et al.* have determined the critical island size independent of nucleation theory for Ag/Pt(111), either by direct measurement of the mean island sizes in the very initial stages of nucleation[8] or by measuring the temperature threshold for Ostwald ripening of dimers.[14] Therefore the rate dependence as well as the Arrhenius behavior of the saturation island density at a known critical cluster size of 1 allowed a direct test of nucleation theory for isotropic substrates.[8] The analysis of nucleation on anisotropic substrates, however, is still in progress.[9,10,12]

The particular bond geometry on square lattices leads to characteristic features in the nucleation kinetics on fcc(100) surfaces. These particularities include the stability of islands. In order to elucidate that, we briefly recall the concept of the critical nucleus. The critical nucleus i corresponds to an island which becomes stable by the incorporation of an extra atom. Here ''stable'' refers to the time scale of deposition; i.e., stable islands have a higher probability to grow than to dissociate. In addition, the islands have to stay stable during the time scale of the measurement. This is usually the case since, after deposition has been terminated, the islands have grown considerably. Depending on substrate temperature, deposition rate, and binding energies, one may find for very low temperatures that the monomers do not migrate at all (statistic growth with monomers being stable, i.e., $i=0$).

With increasing temperature, the monomers start to migrate and to form dimers which are stable ($i=1$). Increasing the temperature further, either the trimer becomes the smallest stable island ($i=2$) or the smallest island corresponds to a tetramer ($i=3$), and so on. This classic continuum model ignores the adsorption site geometry of the substrate, which does not matter for the critical island sizes $i=0$ and $i=1$. The adsorption site geometry, however, becomes important on square lattices when $i=2$. Contrary to triangular or hexagonal surfaces, on square surfaces the dissociation of both dimers ($i=1$) and timers ($i=2$) is characterized by single bond breaking and therefore associated with similar dissociation barriers. Hence, on square lattices, one expects a direct change from $i=1$ to $i=3$ due to the transition from single- to double-bond breaking. The atoms of compact islands which contain four atoms have two next neighbors in the adlayer. Above $i=3$, there is no well-defined behavior since all islands on square lattices are characterized by single- or double-bond breaking. Thus the ''magic'' islands are expected to be the dimer and the tetramer for square symmetry, whereby for hexagonal surfaces the ''magic'' islands might be the dimer, the trimer, and the heptamer.

The purpose of the present work is to verify the well-defined transition from $i=1$ to $i=3$ by the systematic change of substrate temperature and flux. The determination of the sizes of the critical nuclei, of the migration barrier, and the dimer bond energy, as well as the related attempt frequencies, is based on the comparison of the experimental results to mean-field nucleation theory.[1] In addition, we have analyzed the island size distributions in comparison with scaling theory.[15,16] For compact islands, the size distributions fulfill this recently found scaling. The size of the critical nucleus is therefore consistently determined by the scaling behavior of the island size distributions and the rate dependence of the saturation island density.

For low substrate temperatures and, therefore, low migration rates with respect to deposition rate, we have found a plateau in the Arrhenius plot as well as in the rate dependence of the saturation island density. Simulations based on rate equations clearly show that this plateau is a result of postgrowth and postnucleation due to the incorporation of monomers into existing islands and the formation of additional islands *after deposition*.

II. EXPERIMENTAL DETAILS

The growth of copper on Ni(100) has been investigated by means of variable-temperature STM at substrate temperatures between 100 and 400 K; analogous instrumentation as used here has been described in Ref. 17. The nickel crystal was prepared by argon-ion sputtering and subsequent annealing to 1200 K, resulting in nearly perfect terraces of several hundred nanometers. Copper was deposited by thermal evaporation from a Knudsen-type molecular beam epitaxy (MBE) source at a background pressure below 5×10^{-10} mbar. The growth rate has been varied between 5×10^{-5} and 5×10^{-3} monolayers per second (ML/s). It was calibrated from STM images with monolayer coverage. The STM measurements have been performed in the constant current mode at 0.5–2.0 V positive or negative bias and 0.5–8.0 nA tunneling current.

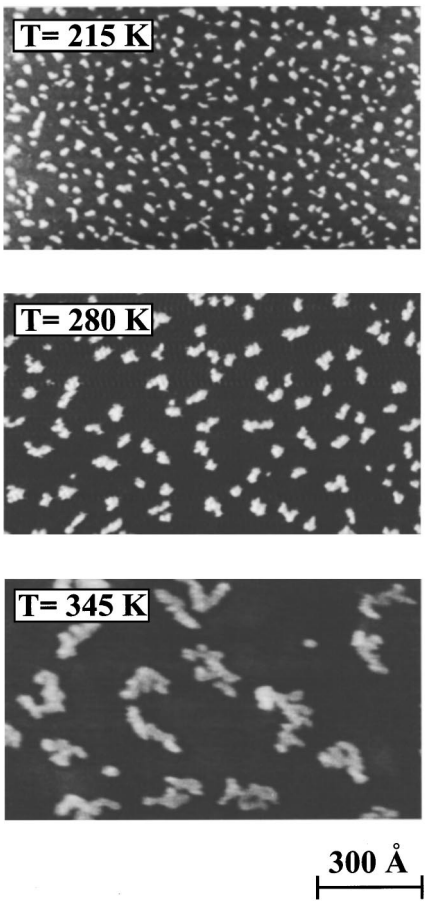

FIG. 1. STM images characterizing the submonolayer growth of Cu on Ni(100) at different growth temperatures. The deposition rate was 1.34×10^{-3} ML/s and the coverage corresponds to about 0.1 ML.

The island densities were determined by counting the islands on a certain area, where the size of the analyzed area has been corrected for thermal drift by determination of characteristic features at successively obtained images. The influence of structural defects such as steps has been excluded by depicting areas far away from such defects.

III. NUCLEATION AND CRITICAL NUCLEUS SIZE

The variation of the saturation island density with substrate temperature is characterized in Fig. 1, showing STM images obtained at 215, 280, and 345 K, respectively. Low substrate temperatures result in high island densities and higher substrate temperatures give considerably lower island densities for a fixed deposition rate. These island densities directly reflect the adatom mobility, which depends exponentially on the substrate temperature. Note that the larger islands in Fig. 1 are rather irregular at high substrate temperatures (215–370 K). This is surprising since it contradicts the generally accepted picture that on square lattices edge diffusion is always fast enough to produce compact and rectangular islands.[18] The physical reason underlying the generation of islands with a noncompact shape at high substrate temperatures is related to a better strain accommodation for

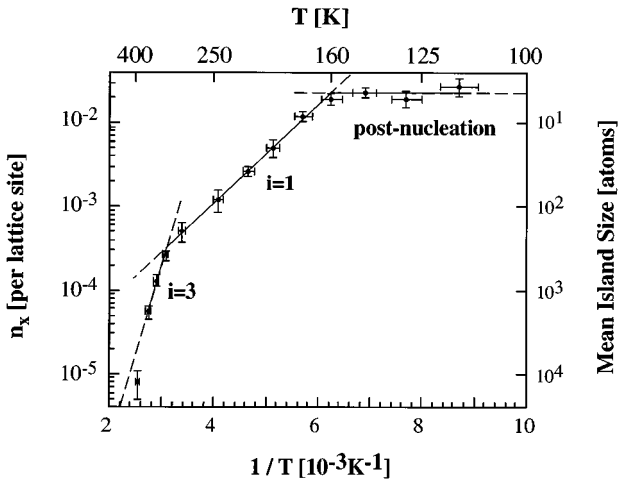

FIG. 2. Arrhenius plot of the measured saturation island density of Cu on Ni(100) (flux 1.34×10^{-3} ML/s, coverage 0.1 ML).

noncompact heteroepitaxial islands; it is quantitatively discussed elsewhere.[19]

In order to get quantitative insight into the microscopic processes which determine the nucleation kinetics for the present system, we have measured the saturation island density (averaging many STM images) as a function of substrate temperature and deposition flux.

Figure 2 shows the measured temperature dependence of the saturation island density as an Arrhenius plot at a coverage of 0.1 ML and a flux of 1.34×10^{-3} ML/s. In the temperature range between 100 and 400 K, the island density as well as the mean island size varies over more than three orders of magnitude. One can clearly distinguish three regions which differ in slope. The different nucleation regimes are labeled postnucleation, $i=1$, and $i=3$, respectively. Below 160 K, the island density does not vary with temperature indicating statistic growth with $i=0$. However, the mean island size of 4–5 atoms is too large, since for statistic growth a mean island size of 1.25 atoms is obtained on a square lattice at 0.1 ML (see Ref. 20 and the discussion of Fig. 5 below). Therefore statistic growth has to be excluded. The physical reason for the plateau in the Arrhenius plot is the island formation and the incorporation of monomers into existing island *after deposition* and will be discussed later, in detail.

The two regimes entered above 160 and 320 K, respectively, have been labeled corresponding to the size of the critical nuclei. In order to establish these sizes, we measured the rate dependence of the island density $n_x(R)$ at three different substrate temperatures 145, 215, and 345 K, each of which is located in the center of the labeled regions in the Arrhenius plot. It is well established from nucleation theory[2] as well as from kinetic Monte Carlo simulations[15,21,22,23] that the rate dependence of the island density follows a power law $n_x\sim(D/R)^{-\chi}$, with χ being 1/3 for $i=1$.[24] The diffusion constant D characterizes the monomer migration at a certain temperature, which is on a square lattice. $D=\frac{1}{4}\nu_0\exp(-E_m/kT)$. For the different critical island sizes, the exponent χ corresponds to $i/(i+2)$ for isotropic two-dimensional (2D) migration;[2] thus, it is 0.5 for $i=2$ and raises to 0.6 for $i=3$.

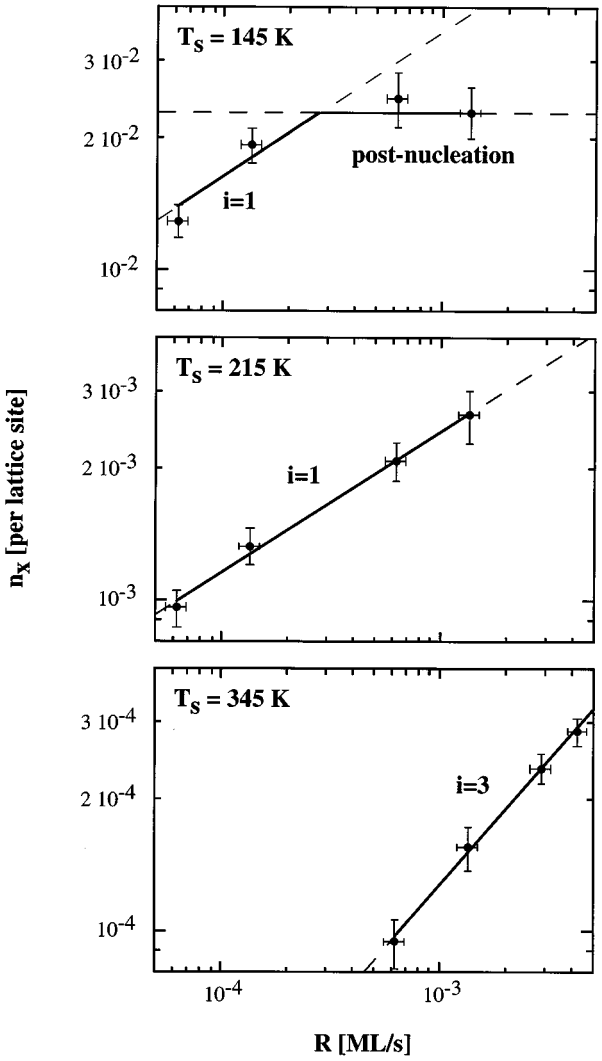

FIG. 3. Double-logarithmic plot of island density vs deposition flux at different growth temperatures in the saturation regime, coverage 0.1 ML.

Double-logarithmic plots of the island density versus flux for the three nucleation regimes are shown in Fig. 3. At 145 K the island density is found to be constant for the higher growth rates due to postnucleation (as discussed in detail below). At 215 K the exponent corresponds to (0.32 ± 0.01), which clearly shows that the monomer is the critical nucleus and the dimer is the smallest stable island ($i=1$). At 345 K the fit yields an exponent of (0.58 ± 0.02), which is in excellent agreement with $i=3$; i.e., the tetramer becomes the smallest stable island. Accordingly, the scaled island size distribution determined for that temperature shows the shape predicted for $i=3$ from scaling theory.[25] The scaled island size distributions at 160 and 215 K are discussed below.

Because the sizes of the critical nuclei are known, the migration barrier of a single adatom E_m and the dimer bond energy E_b as well as the attempt frequency ν_0 can be determined analyzing the Arrhenius plot of the saturation island density in Fig. 2. Copper is known to grow two dimensional on Ni(100), and reevaporation of copper atoms from the surface can be neglected in the considered temperature range 100–400 K. On this basis, i.e., for 2D islands and complete

condensation, the saturation island density n_x is only a function of deposition rate R and substrate temperature T and given for a square lattice[2] by

$$n_x \cong 0.2\left(\frac{4R}{\nu_0}\right)^{i/(i+2)} \exp\left(\frac{1}{(i+2)kT}(iE_m+E_i)\right). \quad (1)$$

In this equation, k is the Boltzmann constant and E_i the binding energy of the critical nucleus i, i.e., $E_0=E_1=0$, $E_2=E_b$, and $E_3\cong 2E_b$. The latter value is based on a bond-counting argument, where E_i is given by the number of nearest-neighbor adatom bonds in the critical nucleus i times the binding energy per bond E_b.

The barrier and attempt frequency, E_m and ν_0, for Cu monomer migration on Ni(100) are obtained in the temperature range where the critical nucleus is 1 (between 160 and 320 K). The slope of the linear fit results in a migration barrier of $E_m=(0.351\pm0.017)$ eV. The attempt frequency is found by the intersection of the linear fit with the ordinate and yields $\nu_0=4\times10^{(11\pm0.3)}$ Hz. The slope of the second linear fit, where $i=3$, then unambiguously determines the dimer bond energy, for which we obtain $E_b=(0.46\pm0.19)$ eV.

As an additional check for the consistency of the foregoing analysis, one can extract the attempt frequency for single-bond breaking from the intersection of the ordinate and the fit to the $i=3$ data. The value $\nu_0^*=5\times10^{(12\pm2)}$ Hz agrees within the error bars to the attempt frequency of monomer migration. If one ignores the result from the flux dependence ($i=3$) and assumes $i=2$ for substrate temperatures above 320 K, one obtains an attempt frequency of $\nu_0^*=5\times10^{(15\pm2)}$ Hz, which is far to high, if one takes into consideration that the attempt frequencies for the different processes are of the same order of magnitude.

Our value of $E_m=(0.351\pm0.017)$ eV for Cu/Ni(100) compares well with other experimental values obtained for migration on fcc(100) surfaces. For Fe/Fe, Stroscio *et al.* derived a slightly higher value of (0.45 ± 0.05) eV from STM inferred island densities between 300 and 530 K.[7,13] For homoepitaxial growth on Cu(100), Dürr *et al.* found from a low-energy electron diffraction (LEED) analysis of island separations as a function of temperature $E_m=(0.36\pm0.03)$ eV,[3] which is quite close to our value. [Note that there are different experimental values in the literature for Cu/Cu(100): 0.28 ± 0.06 eV (Ref. 4) and 0.39 eV (Ref. 26).] From field ion microscopy (FIM) measurements, it is known that migration of single adatoms on fcc(100) surfaces can involve exchange processes [see, e.g., Pt/Pt(100) with a migration barrier of 0.47 eV (Ref. 27)]. This implies the question of whether surface migration of Cu/Ni(100) takes place by exchange or hopping. Since Cu/Ni(100) is a heteroepitaxial system, we can expect to find indications for exchange processes, either upon different imaging of Cu and Ni adatoms (the distinction of different metal atoms within alloyed surfaces by means of STM has been reported several times in the literature; see, e.g., Refs. 28–30) or from a particular nucleation behavior, as, e.g., observed for Fe/Cu(100) (Ref. 31) and Ni/Ag(111) (Ref. 32). Up to substrate temperatures of 400 K, there is no evidence for intermixing in the STM images and the nucleation behavior is in full agreement with migration by hopping on fcc(100). Above 450 K, on the other hand, the step edges appear spotted indicating the onset of alloying. Therefore we conclude, in agreement with a theoretical study,[33] that for Cu/Ni(100) surface migration takes place by hopping in the temperature range investigated here (100–400 K).

Our experimental value for the dimer bond energy $E_b=(0.46\pm0.19)$ eV is relatively large. This explains the sharp transition from $i=1$ to $i=3$ and the well-defined $i=3$ regime, which is not generally expected for nucleation on square lattices.[34] (Using the criterion for the relation of binding energy and transition temperature given in Ref. 35 and a transition temperature of 320 K for $i=1$ to $i=3$, one obtains $E_b=0.35$ eV.) The extended temperature regime in which tetramers are stable can also be explained by the strong lateral bonding. It is interesting to compare our experimental results to calculations performed with effective medium theory (EMT).[36,37] For hopping migration of Cu on Ni(100), we calculate $E_m=0.47$ eV, which is slightly higher than our experimental value; it compares well to the value of 0.45 eV calculated by Perkins and DePristo.[33] For the activation barrier of dimer dissociation, we calculate 0.74 eV, yielding a dimer bond energy of $E_b=0.27$ eV, which is somewhat smaller than the experimental value. In view of the approximate character of EMT and the large error bar of E_b in the experiment, there is reasonable agreement. Recently, a study of the nucleation behavior of Ag/Ag(100) by means of STM in comparison with kinematic Monte Carlo (KMC) simulations revealed a dimer bond energy close to our value of $E_b=0.29$ eV.[38] Since the ratio of E_b to E_m is essential for a sharp transition from $i=1$ to a well-defined $i=3$ behavior, one would also expect such a transition for Ag/Ag(100). For Cu/Cu(100), on the other hand, a surprisingly small (average) dimer bond energy of 0.06 eV has been reported.[3] Based on this value and the arguments outlined above, which are discussed in detail in Ref. 34, a transition from $i=1$ to a well-defined $i=3$ regime is not expected. From the dependence of island separation versus flux, the authors conclude, however, that such a transition occurs.[39] Since the value of E_b is based on this assumption, it should be interpreted with care, as has also been noticed by the authors themselves.[3] In addition, the data are better explained by a transition from hopping to exchange with increasing temperature instead of a transition in critical island size.[40] Moreover, the experimental value is too small compared with theory.[41] A binding energy of 0.20 eV is more realistic.[35] Nevertheless, the lateral bonding of Cu on Cu(100) seems to be much weaker than on Ni(100).

One indication for this behavior is the dependence of the island density on the film thickness during the multilayer growth of copper on Ni(100). For a substrate temperature of 345 K and coverages above 1 ML, we find a substantial decrease in island density with increasing film thickness, in agreement with *in situ* high-resolution low-energy electron diffraction [spot-profile analysis (SPA)-LEED] measurements.[42] The peak intensity of the specular beam shows two oscillations related to the growth of the first and second monolayers. The first minimum is more pronounced than the second one, characterizing a decrease of island density. Above 2 ML, the oscillations vanish, since the multilayer film grows in step flow mode at 345 K. This implies an increasing adatom mobility as the Cu film adopts

copper bulk properties with increasing thickness. The final nucleation kinetics will resemble that of Cu(100). As the migration barriers for copper on Cu(100) and Ni(100) are similar, the difference in island densities is an indication for strongly differing dimer bond energies, i.e., differing critical nuclei.

The particularly strong lateral bonding of Cu on Ni(100), manifested in the large dimer bond energy, might also be one of the main physical reasons for strain relief via internal faceting, which has recently been discovered for this system.[43–45] In this mechanism, the strain in the first monolayer is relieved by translation of atomic rows by half a lattice constant, which locally increases the lateral coordination. This is expected to be especially favorable for a system with strong lateral bond energies.[44]

It is important to mention that for Cu/Ni(100) we were not able to detect any evidence for the migration of small islands. Very recently, it has been suggested that especially tetramers should have a low barrier to migrate via dimer shearing.[46] We believe that the strong lateral bonding is responsible for the absence of this effect for Cu/Ni(100). It should be noted, however, that dimer shearing generates single-bonded atoms in an intermediate state. Whether and how often the single-bonded atom leaves the island, which leads to its dissociation, or the sheared dimer relaxes back to a tetramer determines whether an $i=3$ regime exists at all. Note that the results from embedded-atom method (EAM) in Ref. 46 also imply that for Cu, Ag, and Ni there should be no $i=1$ regime, since the activation energy for dimer dissociation corresponds roughly to the barrier of monomer migration.

It is worth mentioning that the lowest island density we report in Fig. 2 suggests a second transition in critical island size (see deviation of the last point in Fig. 2 from the $i=3$ fit). Relying on the arguments on reasonable attempt frequencies discussed above, our value is compatible with a change from $i=3$ to $i=8$. The data, however, are not conclusive on this; in order to prove such a transition, one would need island densities further below, which are difficult to access due to the finite terrace width.

IV. POSTNUCLEATION

In the following, we discuss nucleation of Cu on Ni(100) in the low-temperature regime ($T<160$ K). At these temperatures and the deposition flux applied for the experiments presented in Fig. 2, adatom diffusion is slow with respect to deposition; therefore, nucleation and growth largely take place after deposition. This regime is called postgrowth. the equilibration of the surface after interruption of deposition has been addressed earlier in context with the growth interruption technique in MBE.[47] This equilibration consists in the smoothening of the surface; it comprises disintegration of, and descend from islands associated with adatom attachment to substrate steps. In variance to this 3D smoothening, we deal with 2D nucleation and growth of islands from monomers, which we therefore call postnucleation. Postnucleation occurs because after the deposition the sample is kept at the same temperature for STM imaging. The effect can be almost suppressed, when the sample is immediately quenched down to 30 K after deposition, because then the remaining monomers are frozen and can subsequently be imaged by STM.[11]

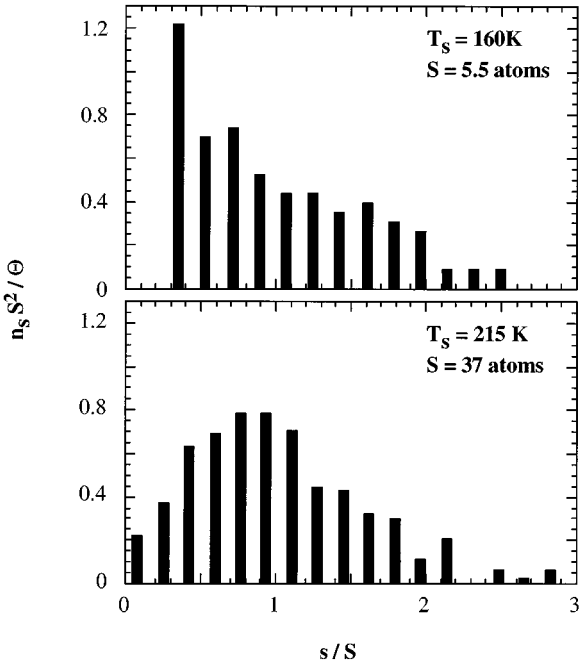

FIG. 4. Scaled island size distributions deduced from STM images at the saturation coverage of 0.1 ML. The Cu deposition flux was 1.34×10^{-3} ML/s. The Ni(100) substrate temperatures and mean island sizes are indicated.

Here we summarize the experimental observations for $D/R<10^4$. First, there is a plateau in the Arrhenius plot for substrate temperatures of less than about 160 K (cf. Fig. 2). Second, we have also found a plateau for the rate dependence of the island density at 145 K (Fig. 3). The crossing of the horizontal line and the line labeled $i=1$ in Figs. 2 and 3 can in both cases be related to $D/R=5\times10^2$. Third, the analysis of the scaled island size distributions at 160 and 215 K results in a totally different behavior (Fig. 4). At 215 K the scaled island size distribution has a maximum of 0.8 and shows clearly that the critical nucleus is a monomer.[13,15,16] This is consistent with the measured exponent of $\chi=\frac{1}{3}$ at this temperature. At 160 K, on the other hand, the scaled island size distribution decreases monotonously in an exponential fashion as has been found for statistic growth ($i=0$).[16] Thus, post-growth results in a behavior very similar to statistic growth; however, the mean island sizes are much larger as a result of monomer mobility. Statistic growth on a square lattice would result in a mean island size of 1.25 atoms at 0.1 ML (see Fig. 5 and Ref. 20), whereas we observe a mean island size of 5.5 at 160 K. At this temperature, postgrowth plays the dominant role, because the monomers are mainly incorporated into islands that have already formed during deposition. For lower temperatures ($T<150$ K), postnucleation becomes more and more important, because an essential amount of monomers forms additional islands after deposition (cf. Fig. 5). Taking account of this difference, we distinguish the post*growth* and the post*nucleation* regimes (see Fig. 6).

These experimental findings can be compared to a rate

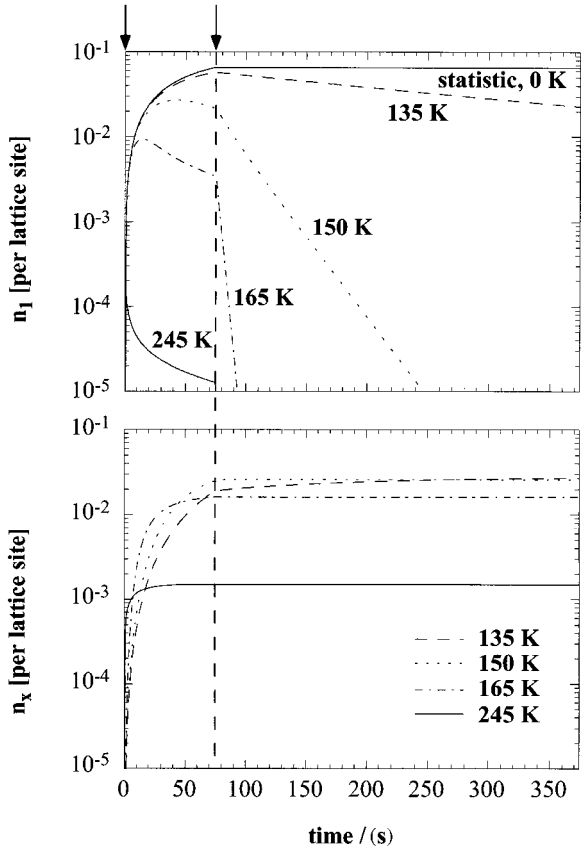

FIG. 5. Monomer density and density of stable islands during and after deposition at different substrate temperatures as computed from rate equations within the lattice approximation (see text). Deposition starts at 0 and is stopped at 75 s corresponding to a coverage of 0.1 ML.

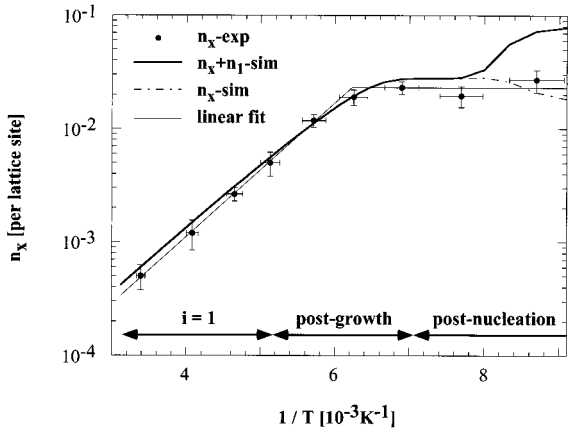

FIG. 6. Comparison of calculated to experimental island densities at 0.1 ML. The transition from dynamic nucleation (with $i=1$) to postgrowth with decreasing temperature is well reproduced by the rate equation analysis. In the postnucleation regime the measured island densities are significantly lower than the ones expected from the calculation of stable islands, n_x, which might be interpreted as an indication for transient mobility.

equation analysis. We take into consideration the regime where the dimer is the smallest stable island ($i=1$) and compute the evolution of the monomer density n_1 and the density of the stable islands n_x as a function of time,[2,8]

$$\frac{dn_1}{dt}=R-2D\sigma_1 n_1^2-D\sigma_x n_1 n_x-R(Rt-n_1)-10Rn_1,$$

$$\frac{dn_x}{dt}=D\sigma_1 n_1^2+5Rn_1-2n_x\left(-\frac{dn_1}{dt}+R\right).$$

The monomer density increases by the deposition rate R (flux). It is reduced by several processes; two monomers form a dimer by migration (second term); a monomer migrates towards a stable island (third term); a monomer is deposited on top of a stable island (fourth term); and on top of another monomer (fifth term), respectively. The factor of 10 in the fifth term accounts for the fact that a dimer is created either when the monomer directly arrives on top of the adsorbed monomer or on one of its four neighboring sites; these five channels have to be doubled since two monomers disappear by the creation of a dimer. The deposition of monomers onto neighboring sites of stable islands is neglected for simplicity. The density of the stable islands, on the other hand, increases by the creation of dimers due to monomer migration (first term of the second equation) and due to the deposition of an atom on top of a monomer and its nearest-neighbor sites (second term). The coalescence reduces the density of stable islands (third term).

These rate equations are solved by numerical integration with a Runge-Kutta algorithm. As an approximation for the capture number σ_x of stable islands, we chose the lattice approximation,[1,48] whereas for monomers we have set $\sigma_1=3$, which is equal to the geometrical concept[49] applied to monomers.[8,11] This assumption for σ_1 considerably simplifies the calculation while still giving reasonably good results. In order to have the same set of rate equations during and after deposition, we introduced a time-dependent deposition rate $R(t)$, which is constant during deposition and zero afterwards. The resulting monomer density as well as the density of the stable islands as a function of time are shown in Fig. 5 on a logarithmic scale. In the first 75 s, 0.1 ML are deposited and then the system is allowed to develop for another 300 s after closing the shutter.

The graph labeled statistic growth corresponds to immobile adatoms ($i=0$). The curve actually shows the result from integrating the rate equations for $T=0$ K, which is almost identical with the result from percolation theory on the square lattice.[20] There is a minor difference, however, which is not apparent in Fig. 5. The monomer density is slightly lower in the rate equation result (less than 5% after closing the shutter), since there atoms impinging on top of adatoms are allowed to descend and to form a dimer, whereas these atoms are removed in percolation theory. The statistic growth is related to the highest possible island density (including monomers as islands). Note that the curve obtained for Cu/Ni(100) at 135 K is still quite close to this regime. With increasing temperature, one can nicely see how the monomer density left after closing the shutter steadily decreases, since an increasing number of islands nucleate and grow already during deposition. The final densities of stable islands are quite similar for $D/R<10^4$, which correspond to substrate temperatures of 135, 150, and 165 K. This result of the simulations is in agreement with the experimen-

tal observed plateau in the Arrhenius plot.

The ratio of surface migration and deposition flux is $D/R=10^3$ at 165 K. In general, postnucleation is expected to be dominant below this threshold. For Ag/Pt(111), e.g., postgrowth has been demonstrated to become important at 65 K, which also corresponds to $D/R=10^3$.[8] The curve in Fig. 5 for a substrate temperature of 245 K, on the other hand, shows the typical dynamic nucleation and growth behavior where nearly all monomers are incorporated during deposition.

All experimentally observed phenomena from dynamic nucleation with $i=1$ to postnucleation discussed above can qualitatively be explained by our rate equation analysis. This is demonstrated in Fig. 6 comparing the measured and calculated island densities as a function of $1/T$. The quantitative agreement between the experimentally observed island densities and the simulated ones is excellent; it may be even improved by a more appropriate choice of capture numbers. The lattice approximation used here results in slightly higher values than the experiment for the dynamical $i=1$ regime, as also found by Bott *et al.*[11]

The solid line in Fig. 6 represents the calculated total island density including the monomers which exist after a wait time of 10^4 s, whereby the dashed line only shows the stable islands, i.e., dimers and larger ones. For the dynamic and the postgrowth regime, the curves are identical. The difference between the n_x+n_1 simulation (solid curve) and the experimental data in the postnucleation regime suggests that atoms upon deposition have an enhanced mobility with respect to equilibrated adatoms at these substrate temperatures; this might be ascribed to transient mobility.[50] Recently, the postgrowth of Cu/Ni(100) has also been studied by means of SPA-LEED.[51] The full width at half maximum (FWHM) of the specula beam directly reflects the mean island size. Thus the decrease of FWHM in time after deposition yields the time constant for monomer depletion which can also be used to determine the migration barrier. Assuming reasonable values for attempt frequency, island density, and captive numbers, one obtains $E_m=(0.41\pm0.04)$ eV in agreement with the analysis above.

V. CONCLUSION

Postgrowth and postnucleation, which show similarities to statistic growth, have been observed and quantitatively discussed for Cu nucleation on Ni(100) for $D/R<10^4$. At a temperature of 320 K, an abrupt transition from $i=1$ to $i=3$ has been demonstrated, and the barrier for monomer migration and the dimer bond energy have been determined.

The post-growth and post-nucleation phenomena are not only interesting from a fundamental point of view, but also of potential technological relevance since in industrial film growth deposition rates are orders of magnitudes higher. Typical growth rates in MBE (1 ML/s) are three orders of magnitude higher than in our experiments, and for laser deposition experiments the rates are up to 8 orders of magnitude higher than the ones discussed here. Therefore postnucleation and postgrowth can play an important role even at high temperatures depending on the D/R ratio. The present study demonstrates that by the use of both experiment and a simple rate equation analysis a detailed understanding of the first stages of epitaxial growth on an atomic scale can be obtained.

ACKNOWLEDGMENTS

We gratefully acknowledge discussions with L. Bürgi on percolation theory who also supplied the numerical solutions to this theory. We are grateful to J. W. Evans and M. C. Bartelt (Ames Laboratory) for valuable discussions. We would also like to thank J. Jacobsen, K. W. Jacobsen, P. Stoltze, and J. Nørskov (DTU Denmark) for making available the EMT code to us. Financial support of the Alexander von Humboldt-Stiftung (B.M.) and the Deutscher Akademischer Austauschdienst (L.N.) is gratefully acknowledged.

[1] J. A. Venables, Philos. Mag. **17**, 697 (1973).
[2] J. A. Venables, G. D. T. Spiller, and M. Hanbücken, Rep. Prog. Phys. **47**, 399 (1984).
[3] H. Dürr, J. F. Wendelken, and J. K. Zuo, Surf. Sci. **328**, L527 (1995).
[4] H. J. Ernst, F. Fabre, and J. Lapujoulade, Phys. Rev. B **46**, 1929 (1992).
[5] M. Bott, T. Michely, and G. Comsa, Surf. Sci. **272**, 161 (1992).
[6] H. Röder, H. Brune, J. P. Bucher, and K. Kern, Surf. Sci. **298**, 121 (1993).
[7] J. A. Stroscio, D. T. Pierce, and R. A. Dragoset, Phys. Rev. Lett. **70**, 3615 (1993).
[8] H. Brune, H. Röder, C. Boragno, and K. Kern, Phys. Rev. Lett. **73**, 1955 (1994).
[9] J. P. Bucher, E. Hahn, P. Fernandez, C. Massobrio, and K. Kern, Europhys. Lett. **27**, 473 (1994).
[10] S. Günther, E. Kopatzki, M. C. Bartelt, J. W. Evans, and R. J. Behm, Phys. Rev. Lett. **73**, 553 (1994).
[11] M. Bott, M. Hohage, M. Morgenstern, T. Michely, and G. Comsa, Phys. Rev. Lett. **76**, 1304 (1995).
[12] T. R. Linderoth, J. J. Mortensen, K. W. Jacobsen, E. Laegsgaard, I. Stensgaard, and F. Besenbacher, Phys. Rev. Lett. **77**, 87 (1996).
[13] J. A. Stroscio and D. T. Pierce, Phys. Rev. B **49**, 8522 (1994).
[14] H. Röder, E. Hahn, H. Brune, J. P. Bucher, and K. Kern, Nature (London) **366**, 141 (1993).
[15] M. C. Bartelt and J. W. Evans, Phys. Rev. B **46**, 12 675 (1992).
[16] J. G. Amar and F. Family, Phys. Rev. Lett. **74**, 2066 (1995).
[17] H. Brune, H. Röder, K. Bromann, and K. Kern, Thin Solid Films **264**, 230 (1995).
[18] Z. Zhang, X. Chen, and M. G. Lagally, Phys. Rev. Lett. **73**, 1829 (1994).
[19] B. Müller, B. Fischer, L. Nedelmann, H. Brune, and K. Kern (unpublished).
[20] M. F. Sykes and M. Glen, J. Phys. A **9**, 87 (1976).
[21] M. C. Bartelt and J. W. Evans, Europhys. Lett. **21**, 99 (1993).
[22] G. S. Bales and D. C. Chrzan, Phys. Rev. B **50**, 6057 (1994).
[23] J. W. Evans and M. C. Bartelt, J. Vac. Sci. Technol. A **12**, 1800 (1994).
[24] Strictly speaking, $\chi=\frac{1}{3}$ is only exact for compact islands. For

ramified islands slightly higher values have been reported in Ref. 22.
[25] B. Müller, L. Nedelmann, B. Fischer, H. Brune, and K. Kern, in Surface Diffusion: Atomistic and Collective Processes, edited by M. Scheffer and M. C. Trimgides, NATO Advanced Study Institute, Series B; Physics (Plenum, New York, in press).
[26] M. Breeman and D. O. Boerma, Surf. Sci. **269/270**, 224 (1992).
[27] G. L. Kellogg, Surf. Sci. Rep. **21**, 1 (1994).
[28] M. Schmid, H. Stadler, and P. Varga, Phys. Rev. Lett. **70**, 1441 (1993).
[29] H. Röder, R. Schuster, H. Brune, and K. Kern, Phys. Rev. Lett. **71**, 2086 (1993).
[30] D. D. Chambliss and S. Chiang, Surf. Sci. Lett. **264**, L187 (1992).
[31] D. D. Chambliss and K. E. Johnson, Phys. Rev. B **50**, 5012 (1994).
[32] J. A. Meyer and R. J. Behm, Surf. Sci. **322**, L275 (1995).
[33] L. S. Perkins and A. E. DePristo, Surf. Sci. **319**, 225 (1994).
[34] M. C. Bartelt, L. S. Perkins, and J. W. Evans, Surf. Sci. **344**, L1193 (1995).
[35] J. W. Evans and M. C. Bartelt, in Ref. 25.
[36] K. W. Jacobsen, Comments Condens. Matter Phys. **14**, 129 (1988).
[37] P. Stoltze, J. Phys. Condens. Matter **6**, 9495 (1994).
[38] C.-M. Zhang, M. C. Bartelt, J.-M. Wen, C. J. Jenks, J. Evans, and P. A. Thiel, J. Cryst. Growth (to be published).
[39] J. K. Zuo, J. F. Wendelken, H. Dürr, and C. L. Liu, Phys. Rev. Lett. **72**, 3064 (1994).
[40] I. Markov, in Ref. 25.
[41] C. L. Liu, Surf. Sci. **316**, 294 (1994).
[42] L. Nedelmann, B. Müller, B. Fischer, K. Kern, D. Erdös, and J. Wollschläger (unpublished).
[43] B. Müller, B. Fischer, L. Nedelmann, A. Fricke, and K. Kern, Phys. Rev. Lett. **76**, 2358 (1995).
[44] B. Müller, B. Fischer, L. Nedelmann, H. Brune, and K. Kern, Surf. Rev. Lett (to be published).
[45] B. Müller, L. Nedelmann, B. Fischer, A. Fricke, and K. Kern, J. Vac. Sci. Technol. A **14**, 1 (1996).
[46] Z. P. Shi, Z. Zhang, A. K. Swan, and J. F. Wendelken, Phys. Rev. Lett. **76**, 4927 (1996).
[47] S. Harris and P. Smilomer, Phys. Rev. B **50**, 7952 (1994); Refs. 22 and 23 therein.
[48] M. J. Stowell, Philos. Mag. **26**, 349 (1972).
[49] G. Zinsmeister, Thin Solid Films **7**, 51 (1971).
[50] W. F. Egelhoff and I. Jacob, Phys. Rev. Lett. **62**, 921 (1989).
[51] J. Woleschläger, D. Erdös, L. Nedelmann, B. Fischer, J. V. Barth, B. Müller, and K. Kern (unpublished).